PCCP
INVITED ARTICLE

Exact reaction dynamics by the hyperquantization algorithm: integral and differential cross sections for $F + H_2$, including long-range and spin–orbit effects

V. Aquilanti,[a] S. Cavalli,[ab] D. De Fazio,[a] A. Volpi,[a] A. Aguilar,[c] X. Giménez[c] and J. M. Lucas[c]

[a] *Dipartimento di Chimica, Università di Perugia, 06123 Perugia, Italy*
[b] *Istituto Nazionale di Fisica della Materia (INFM), Unitá di Perugia, 06123 Perugia, Italy*
[c] *Departament de Química Física, Universitat de Barcelona, 08028 Barcelona, Spain*

Received 9th August 2001, Accepted 19th November 2001
First published as an Advance Article on the web 15th January 2002

We present in this article a numerical investigation of the dynamics of the prototypical exchange reaction $F + H_2 \rightarrow HF + H$ applying an exact quantum mechanical method, the hyperquantization algorithm, which exploits discrete analogs of hyperspherical harmonics and whose accuracy is tested for both differential and integral cross sections. The calculations employ the potential energy surface by Stark and Werner, both in its original version (SW PES) and in two new versions, properly adapted to include the effects of the long-range interaction in the reactants' valley (SW-LR) and also those due to the spin–orbit interaction (SW-LR-SO). The features of the potential surfaces in the entrance channel have been modeled according to experimental information coming from total cross section measurements carried out in our laboratory. Computed integral and differential cross sections for H_2 in its ground vibrational state and for rotational states equal to 0, 1, 2 and 3 in the collision energy range 1.8–3.4 kcal mol^{-1} are compared with previous results by other accurate quantum mechanical methods (J. F. Castillo, B. Hartke, H.-J. Werner, F. J. Aoiz, L. Bañares and B. Martínez-Haya, *J. Chem. Phys.*, 1998, **109**, 7224; M. H. Alexander, D. E. Manolopoulos and H.-J. Werner, *J. Chem. Phys.*, 2000, **113**, 11 084) and with several sets of experimental data (differential cross sections (D. M. Neumark, A. M. Wodtke, G. N. Robinson, C. C. Hayden and Y. T. Lee, *J. Chem. Phys.*, 1985, **82**, 3045), nascent rovibrational distributions (W. B. Chapman, B. W. Blackmon, S. Nizkorodov and D. J. Nesbitt, *J. Chem. Phys.*, 1998, **109**, 9306) and total integral cross sections (F. Dong, S.-H. Lee and K. Liu, *J. Chem. Phys.*, 2000, **113**, 3633)) to emphasize the role of intermediate and long-range forces on reaction dynamics. The effect of the modifications of the ground surface due to spin–orbit interaction is also discussed and perspectives for future improvements are pointed out, the main indication being that the effective reaction barrier appears to be lower with respect to that of the original SW PES.

I. Introduction

The exact quantum mechanical treatment of the $F + H_2$ reaction is considered in this article. Since details of old experimental data on this reaction appear to be still waiting for an explanation and new ones are becoming available, this reaction continues to remain under the focus of theoretical treatments. In this paper, numerical results are obtained by a time-independent technique (the hyperquantization algorithm), a main motivation being to exhibit its capability of giving converged integral and differential cross sections.

Comparison between theory and experiments requires a realistic description of the relevant interactions. An important feature of the fluorine atom as a reactant is its open-shell nature and the presence of fine-structure splitting (Fig. 1). In order for the quantum dynamics to be studied accurately, the role of effects such as the long-range behaviour of the potential energy surface and specifically of the spin–orbit coupling in the entrance channel, has to be assessed. The present calculations will be shown to contribute to a better understanding of this role and to point out remaining inaccuracies in current descriptions of the interactions, specifically in the transition state region.

A. The reaction $F + H_2 \rightarrow HF + H$

The reader can appreciate the progress made in the study of reaction dynamics by referring to earlier accounts[1,2] of the reaction $F + H_2 \rightarrow HF + H$. This reaction has a long history in reaction dynamics and extensive attempts were made in order to understand this system at an increasing level of detail. The main motivation is its experimental and theoretical accessibility, which makes it a prototype system for the study of exothermic exchange chemical reactions. Because of the large number of published papers, we will review only the most recent ones needed to appreciate the state-of-the-art for this system.

One of the key experiments to understand the dynamics of this reaction and its isotopic variants was the crossed molecular beam experiment by Neumark and co-workers,[3,4] which provided vibrationally resolved product angular distributions and relative vibrational populations at different collision energies. This experiment confirmed the interesting feature of this reaction, that the vibrational populations of the products are highly "inverted" with a large fraction in the $v' = 2$ vibrational state (for a review see ref. 5), and a selective forward scattering in the $v' = 3$ vibrational level, while most of the

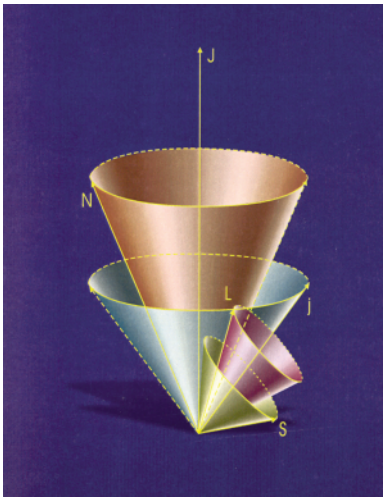

Fig. 1 A vector model illustration of the angular momenta involved in collisions of an atom such as fluorine, having both spin–orbit and open-shell structure. Atomic spin S and electronic angular momenta L (1/2 and 1 respectively for F) add to give j, which for fluorine is 3/2 for the ground state and 1/2 for the first excited state. In a collision j can couple with the orbital angular momentum N to yield a total J. For the $F + H_2$ reaction, further contribution comes from the molecular rotation of hydrogen, also denoted j in the text (for further details, see ref. 47).

products are completely scattered in the backward direction. These findings have received much attention also for the possibility they offer of being exploited in the pumping mechanism for the HF chemical laser.[6]

The challenge for theoreticians was to reproduce these features computationally. It was not clear whether the initial failures were due to the breakdown of the approximations introduced in the treatment of the reaction dynamics or to inadequacies of the potential energy surface (PES). In 1990 the first fully converged quantum calculations on this system were performed by Launay and Le Dourneuf[7] on the most accurate PES available at the time.[8] The inversion of the product vibrational states was reproduced but the $v' = 3$ vibrational level came out more populated than the $v' = 2$. Also, the product angular distribution[9,10] was qualitatively reproduced with the appearance of the selective $v' = 3$ forward scattering, but the height of the peak was overestimated by about one order of magnitude with respect to the experiments.

In the light of these results many attempts were devoted to refining the potential energy surface in order to quantitatively reproduce the experimental findings. New *ab initio* calculations were performed and new PESs, semi-empirical or fully empirical, were constructed. *Ab initio* calculations typically predicted a reaction barrier of about 1 kcal mol^{-1} [8,11] strongly constrained in the linear configuration by a tight bending potential. As for the height of the barrier, there was a serious disagreement among the various calculations and in the last twenty years it has been reported as ranging from 1.6[12] to 3.2 kcal mol^{-1},[13] most rate constant experiments appearing to give credit to the lower values. It began to be clear that the computation of the electronic structure for this elusively simple system was actually a serious and even frustrating problem.[1]

Because of the difficulties encountered by the *ab initio* calculations various empirical approaches were proposed. In such cases the PESs contain parameters which can be optimized to get better agreement with the experiments. Even if dynamical tests were performed with approximate treatments, the prevailing indication was that the reaction transition state was less collinearly constrained, until the appearance, in the empirical Takayanagi and Sato surface,[14] of a bent transition state. In that work it was shown that a bent transition state was also able to give a forward $v' = 3$ peak in classical trajectory calculations, casting serious doubts on its interpretation (currently accepted at the time) as a quantum mechanical resonance. Actually, indications of a bent transition state had been given for the first time by Truhlar's group, combining *ab initio* calculations and a semi-empirical scaled external correlation technique.[15–17] Although these PESs allowed better descriptions of experimental findings[18] with respect to the previous ones, they were not able to provide quantitative agreement, even when empirical parameters were included[19] and dynamical tests were performed with accurate quantum mechanical codes.

A basic contribution to the characterization of the transition state for the $F + H_2$ reaction was published in 1996 by Stark and Werner (SW).[20] In that paper a completely *ab initio* PES was calculated using the internally contracted multireference configuration interaction method (MRCI) with complete active space self-consistent field (CASSCF) reference functions and a very large basis set. Davidson correction was applied. The results of this calculation were a barrier height of 1.84 kcal mol^{-1} for the linear configuration, but the actual saddle point was found to have a bent structure near 60° with a barrier height of 1.45 kcal mol^{-1}. Other critical points were computed and two van der Waals wells were found in the perpendicular and linear configurations of the entrance and exit channels, respectively. The well depths were 0.37 kcal mol^{-1} for the perpendicular one and 0.28 kcal mol^{-1} for the linear one. Quantum mechanical calculations[21,22] performed on this surface accounted for the relative positions and intensities of the peaks in the FH_2^- photoelectron spectrum measured in the experiment of Neumark and co-workers,[23,24] supporting the reliability of this surface in the transition state region. Further refinements of this PES will be discussed at length in Section II.B.

Detailed fully converged quantum mechanical calculations and classical trajectory studies of the reaction dynamics on the SW surface were carried out by Castillo and Manolopoulos[25] and by Aoiz and co-workers,[26] respectively (further dynamical calculations on this PES will be cited below). In those papers the reactants' rotational distribution of the Neumark and co-workers' experimental fluorine beam was simulated to get differential cross sections in the center-of-mass reference frame as well as in the laboratory frame,[27] vibrational branching ratios were also obtained. In both quantum and classical calculations most qualitative features of the experiments were reproduced but for some aspects the agreement was not satisfactory. The largest disagreement with experiment was again found for the highest vibrational level $v' = 3$ of the products. Even if for the first time the yield of $v' = 3$ was found to be smaller than that for $v' = 2$, the quantum mechanical results underestimated their ratios by a factor of up to two and the prediction on the forward peak, even if substantially improved with respect to the preceding quantum calculations, remained unsatisfactory. In particular, modeling of the dynamics by classical trajectories was found to underestimate the forward scattering, while quantum calculations predicted a more pronounced peak than measured.

In ref. 25 (see also ref. 2 for an account of the results obtained on the SW PES) much effort was devoted to characterize the nature of this selective forward peak and, in particular, to verify the hypothesis that this was a manifestation of a quantum mechanical resonance in the $F + H_2$ reaction, which had also been the original proposal by the discoverers themselves.[3] From these studies the correlation between scattering involving high partial waves and the appearance of the forward peak in the differential cross sections has been carefully assessed: the forward peak was clearly attributed to tunneling through the combined effect of both centrifugal and potential reaction barriers at high initial orbital angular momenta and for this reason it is underestimated by classical trajectory approximate treatments of the dynamics. Some doubts still

remain about the possibility that this mechanism can be enhanced by a quantum mechanical shape-resonance. Indications for both the resonance and the direct scattering mechanisms were encountered, even if the authors of ref. 25 seemed inclined to believe to the dominance of the latter. Recently, more detailed investigations on the nature of the forward peak[28,29] confirm a resonance contribution, so preventing definite conclusions on this problem.

The limitations of the SW PES have been further pointed out in the reactive calculations of the F + HD variant, for which fully converged quantum mechanical calculations[30] do not reproduce satisfactorily the recent beam experiments by Dong and co-workers.[31] In fact, even if the total reactive cross section dependence on the energy of the DF channel was well reproduced, the height of the peak of the HF channel was clearly overestimated by a factor of about two. The obvious open question is why the SW surface cannot accurately reproduce all the features of the available experimental scattering data.

Witnessing the continuing interest about the details of this reaction, new experiments at a higher level of accuracy with respect to Neumark's one have been performed in the last few years. Rotationally resolved integral cross sections have been extracted for the first time from molecular beam experiments by Faubel and co-workers[32–34] for the $F + D_2$ reaction, and by Nesbitt's group[35,36] for $F + H_2$ (actually, rotationally resolved differential cross sections for this reaction had been measured before,[37,38] but the experiment was sensitive only to a few rovibrational quantum states of the products and only a few collision energies were selected). An approximate comparison of Nesbitt's experimental results with theoretical data[25] (calculations were performed at a slightly different collision energy) has again indicated disagreement between theory and experiment, especially for the rotational distribution of the $v' = 3$, where theoretical predictions were significantly "colder" than experimental ones. Moreover a small fraction of products were found in the $j' = 5$ rotational state of the $v' = 3$ level, which is closed in the SW surface (inaccurate in the asymptotic product region) but energetically permitted according to the correct thermochemistry.

B. Motivation and plan of the paper

It is commonly accepted that the transition state of the PESs is the most important region in order to reproduce the dynamical properties of a system, and must be characterized with high accuracy. However, it is also clear that even the long-range portions of the interaction, such as the van der Waals wells, can influence the reaction dynamics, by affecting the reactive and inelastic fluxes and by inducing a variable asset to the approach geometries. Evidences for this have been found for the Cl + HD reaction, where the simple introduction of a long-range van der Waals well for the perpendicular configuration drastically changes the products branching ratios, favouring one reaction channel over the other.[39]

In our laboratory, elastic plus inelastic integral cross sections were measured in a magnetically selected fluorine-atom beam experiment for the $F + H_2$[40] and the $Cl + H_2$[41] systems. From the analysis of the "glory" structure of the total integral cross sections, an accurate characterization of the long-range isotropic interaction between the incoming atom and the H_2 molecule has been obtained.

Recently,[42] we have extended the work of ref. 40 and 41 to determine the anisotropic part of the potentials for the ground as well as for the excited electronic states. In our work the potential was expanded in linear combination of the products of two spherical harmonics. One set of harmonics describes the different orientations of the half-filled p orbital of the open-shell fluorine atom and the other set describes the orientation of the H_2 molecule. Each radial term of the expansion was put into relationship with a specific component of the physical interaction and determined from experimental data and from correlation formulas.

This method is expected to be reliable in the intermediate and long-range interaction regions. It allows the spin–orbit interaction to be consistently introduced, and ground and excited surfaces are obtained simultaneously and at the same level of accuracy. However, these surfaces, obtained from total (elastic plus inelastic) cross section measurements, apply only to the entrance channel of the reaction. Complete potential energy surfaces, which allow the reactive path to be open, have been proposed by merging the long-range potentials of ref. 42 with the SW PES. The PES obtained by merging our surface accounting only for the van der Waals well and for electrostatic interaction will be denoted in the following as SW-LR, while the spin–orbit corrected surface correlating with the state $^2P_{3/2}$ of F atom will be indicated as SW-LR-SO. Both can be merged to the spin-free SW PES because in the region where this merging is performed (see section II) the spin–orbit interaction is quenched. This feature diversifies the problem from that of symmetric reactions, such as that of Cl with HCl,[43] for wich the atomic spin–orbit splitting can be assumed constant for all configurations.

In this paper the effects on the reaction dynamics of the long-range part of the potential (SW-LR) as well as of the spin–orbit correction on the ground electronic state (SW-LR-SO) will be examined in detail.

As for the dynamical method, an original hyperspherical technique[44] has been developed by us to solve the three-body reactive scattering problem (see ref. 45 for a presentation of our *hyperquantization algorithm*).[44] This algorithm has been successfully implemented to calculate fully converged quantum mechanical cross sections for the $He + H_2^+ \rightarrow HeH^+ + H$ reaction on a new and accurate *ab initio* potential energy surface.[46] The theory of the algorithm has also been extended to solve the multisurface problem (in ref. 47 the theory and some numerical results are presented). In this paper the hyperquantization algorithm is used to calculate state-to-state integral and differential cross sections on the three different potential energy surfaces mentioned above: the SW PES,[20] the long-range corrected SW-LR PES and the long-range plus spin–orbit corrected SW-LR-SO PES. Detailed comparisons have been made in order to investigate the role of each of the modifications introduced to the original SW PES. Results have been also compared with previous calculations,[25] to verify the accuracy of the dynamical calculations and to compare the effects of the spin–orbit correction.[48,49] The rotational populations of the various experimental beams are also simulated, to directly compare our results with experimental data.[3,31,36]

The scheme of this article is as follows. The modifications of the SW surface in the entrance valley according to our results of ref. 42 as well as the introduction of the spin–orbit effect are described in Section II. Section III is concerned with the numerical details of the calculations by the hyperquantization algorithm. Our results are presented and discussed in Section IV. Conclusions are summarized in the final Section V.

II. Potential energy surfaces

A. The entrance channel

Given that the transition state region of the SW surface is accurate enough to describe successfully the photodetachment experiment,[23,24] the reasons for its shortcomings must be looked for in other features of the surface. A clear indication for this comes from inelastic cross section calculations, which are obviously very sensitive to the long-range portion of the interaction and to the anisotropy of the entrance channel. Various attempts have been made[18,50,51] to introduce the long-range region characterized by our experiments of ref. 40 to

build a realistic potential energy surface for the $F + H_2$ system which was able to describe accurately the inelastic cross section measurements as well as the reactivity of the system.

Since 1993 rotationally resolved differential inelastic cross sections were measured by Faubel and co-workers[50–52] for some rotational transitions of $F + H_2$ and its isotopic variants, and compared with available theoretical treatments. The isotropic part of the potential was taken directly from ref. 40 while the anisotropic part (which is critical to describe the dynamics of the inelastic process) was estimated according to phenomenological models. In these models either a second order truncated Legendre polynomial expansion or a simple scaling of the isotropic part of the potential between linear and perpendicular configurations was performed to simulate the correct anisotropy of the system. The average over the possible orientation of the molecule was imposed to be consistent with ref. 40. The resulting van der Waals region of the PES was directly compared with other surfaces[18] taking into account the same isotropic average. In the van der Waals region the surface of ref. 18 shows two different wells separated by a small barrier with the linear configuration considerably more stable than the perpendicular one. This contradicts the model suggested in ref. 50 and 51, which predicts only one well in the perpendicular configuration. In qualitative agreement with this model, the SW surface predicts a T-shape van der Waals well. Indeed dynamical inelastic calculations on the SW surfaces[52] have given poor agreement with the experimental results, demonstrating that the SW surface is not quantitatively accurate in the entrance channel region, even if it must be recognized that the errors introduced by the approximations in these semi-classical and quantum dynamical calculations leave some doubts about these conclusions (only in ref. 51 was an accurate study of the dynamical uncertainty performed).

However the potential energy surface by Stark and Werner is probably the most accurate existing PES in the transition state region. The idea of this work is to modify the SW surface in the entrance channel of the reaction following our semi-empirical results reported in ref. 42 and to explicitly introduce the orientational anisotropy of the hydrogen molecule, improving on previous work.[42]

We recall here some concepts about the surface representations of ref. 42, which will be adopted here for dynamical calculations. The interaction potential is a function of the Jacobi vector length R, giving the distance between the F atom and the center-of-mass of the H_2 molecule, and of the relative orientation of the half-filled orbital axis and of the molecule, and has been expanded in a series of bipolar harmonics. The latter simulate the angular behavior, while each radial coefficient of the expansion accounts for a specific component of the interaction (dispersion, induction, electrostatic, charge-exchange ...):

$$V(R, r, \hat{r}, \hat{r}_e) = \sum_{l_1, l_2, l_{12}} V^{l_{12}}_{l_1 l_2}(R, r)\, \mathcal{Y}^{l_{12}0}_{l_1 l_2}(\hat{r}, \hat{r}_e) \qquad (1)$$

Here the bipolar harmonics $\mathcal{Y}^{l_{12}0}_{l_1 l_2}$ are a linear combination of normalized spherical harmonics:

$$\mathcal{Y}^{l_{12}0}_{l_1 l_2}(\hat{r}, \hat{r}_e) = \sum_{\mu} \langle l_1 l_2 \mu - \mu \mid l_{12} 0\rangle\, Y_{l_1 \mu}(\hat{r})\, Y_{l_2 - \mu}(\hat{r}_e) \qquad (2)$$

where $\langle ....|..\rangle$ is a Clebsch–Gordan coupling coefficient. $Y_{l_2 \mu}$ are spherical harmonics depending on the orientation $\hat{r}_e$ of the half-filled orbital of the F atom. For a P-state atom, only the coefficients $l_2 = 0, 2$ contribute to the potential energy surfaces.[53] As a consequence, μ values are restricted to 0, 1 and 2. $Y_{l_1 \mu}$ is a spherical harmonic describing the dependence on the orientation $\hat{r}$ of the hydrogen molecule. For H_2, an expansion with $l_1 = 0, 2$ is sufficient to represent asymptotically the molecular anisotropy in the reactant channel.[54,55] The invariance of the potential energy surfaces under the inversion of all the coordinates limits the expansion to even values of $l_1 + l_2 + l_{12}$. As a consequence, l_{12}, corresponding to the coupling of the first two, is also even. The coefficients $V^{l_{12}}_{l_1 l_2}$ in eqn. (1) are parametric in R and r. In ref. 42, we illustrated the case where the molecular internuclear distance r is frozen at the equilibrium value (0.74 Å for H_2). This restriction is amended below.

The radial coefficients in eqn. (1) can be directly estimated from our total cross section measurements and/or calculated by correlation formulas which provide the main features of each interaction component in terms of fundamental physical properties of the interacting partners. For their explicit parametric expressions, see ref. 42. In particular the V^4_{22} term responsible for the quadrupole–quadrupole component of the interaction has been found to be very important to characterize the anisotropy of the Van der Waals well for the perpendicular configuration. The matrix representation of the potential has been obtained first using a p-orbital spin-free basis set of the F atom [compare eqn. (14) in ref. 42]:

$$V_{00}\,\mathbf{1} + \frac{1}{5}\begin{pmatrix} 2V_{20} & \sqrt{6}V_{21} & 0 \\ \sqrt{6}V_{21} & -V_{20} + \sqrt{6}V_{22} & 0 \\ 0 & 0 & -V_{20} - \sqrt{6}V_{22} \end{pmatrix} \begin{matrix} p_z \\ p_x \\ p_y \end{matrix} \qquad (3)$$

where we define

$$V_{l_2 \mu}(R, \hat{r}) = \sum_{l_1 l_{12}} \langle l_1 l_2 \mu\ -\mu \mid l_{12} 0\rangle\, V^{l_{12}}_{l_1 l_2}(R)\, Y_{l_1 \mu}(\hat{r}) \qquad (4)$$

By diagonalizing the matrix (3), the lowest eigenvalue represents, for each nuclear configuration, the ground potential energy surface accounting only for the van der Waals and electrostatic interaction (shape of the long-range potential well). This surface, just like the SW one, asymptotically correlates with the ^2P state of the F atom, the statistically mixed state of the physical $^2P_{3/2}$ and $^2P_{1/2}$ levels. This permits the merging with the SW surface (to be described next) to obtain the PES denoted as SW-LR.

B. The spin–orbit interaction

In the $F + H_2$ dynamics the spin–orbit interaction is one of the mechanisms permitting the coupling between ground and excited electronic states. The doublet P character of the F atom involves the splitting of the atomic level into two states corresponding to different values of the total atomic angular momentum, precisely 3/2 and 1/2 for the ground and for the excited state, respectively (see Fig. 1). The splitting between the two states is only 50.1 meV (1.16 kcal mol^{-1}), so that, at least in the entrance channel, the coupling between the two states cannot be neglected *a priori*. The energy of excited spin–orbit states increases so rapidly as the internuclear distance becomes smaller that, in the transition state region, couplings among the surfaces can be neglected. However, the effects of spin–orbit coupling are certainly manifest in the entrance channel because the asymptotic energy of the lowest surface is decreased by 0.39 kcal mol^{-1} (one third of the spin–orbit separation). Recently, Nizkorodov and co-workers[56] observed some reactivity from the two spin–orbit states $j = 3/2$ and $j = 1/2$ of the fluorine atom, by monitoring selectively individual product rovibrational levels energetically inaccessible for the ground state. Since these levels correlate with the ground potential energy surface, this can be taken as an experimental evidence of the role of spin–orbit coupling between different electronic states.

Two different possibilities have to be considered. The first is that non-adiabatic (anti Born–Oppenheimer), spin–orbit, Coriolis and rotational couplings are strong enough to couple ground and excited surfaces. In this case, only an electronically non-adiabatic formulation of the dynamical problem can give an accurate comparison with the experimental results. The second possibility is that the Born–Oppenheimer separation is

accurate enough to solve the triatomic dynamics restricted to the ground surface. Also in this latter case, however, where couplings among the surfaces are neglected, the spin–orbit influences the dynamical calculations because the barrier increases by 0.39 kcal mol^{-1}, so that we can expect the spin–orbit coupling to give rise to some effects, even if it is not strong enough to modify drastically the reaction dynamics. In such cases an electronically adiabatic dynamical calculation taking into account only the effects of the modification of the ground state can be accurate enough and, in this spirit, much theoretical work has been carried out with an interesting history of its own. Again, only the most recent key references will be taken into account here. Subsequent to the SW PES publication, another potential energy surface of the ground state containing the *ab initio* spin–orbit corrections was published by Hartke and Werner.[49] In that work spin–orbit contributions were included in the entrance channel to the adiabatic SW PES to give the potential energy surface which in the following will be referred to as HSW PES. The main consequence of the spin–orbit correction was an increase of the barrier height by 0.39 kcal mol^{-1} and a decrease in the depth of the van der Waals well by a factor of about two. Using this new PES an even better agreement with the photodetachment experiment of Neumark and co-workers[23,24] has been found. Because of this promising result, it has been believed in the scientific community that the discrepancies between theory and experiments could be explained by proper inclusion of the spin–orbit correction in the ground surface.

A meticulous series of comparisons between theoretical results and many available experimental scattering data sets was performed on the HSW PES by Castillo *et al.*[48] The surprising result has been that introducing the spin–orbit interaction on the ground surface, the general agreement is found to be not better, and sometimes even worse, with respect to the results on the original SW PES. This trend is even more evident in thermal rate constant calculations[57] where the use of the spin-corrected surface clearly underestimates the experimental values while the uncorrected surface appears to give better agreement.[57,58] Actually the reaction rate constants were calculated in ref. 57 using the adiabatic rotational approximation but detailed comparisons with the exact results[59] have shown that this approximation gives accurate integral cross sections for reactions of both Cl and F with H_2. The exact reactive scattering calculations using the original SW surface seem to agree better with the experimental results. The conclusions of that work[57] were that probably the energy of the transition state in the SW surface is overestimated, so that the barrier becomes too high when the proper asymptotic states are taken into account.

Many efforts have been devoted to an electronically non-adiabatic formulation of the $F + H_2$ dynamical problem, treated for the first time for the case of inelastic collisions in a series of papers in the middle of the 70s.[60–62] Some of these calculations[63,64] predicted too strong effects of the spin–orbit or multi-surface couplings on the reactive dynamics, although this could be due to the drastic approximations adopted in introducing the excited surfaces and/or in the dynamical treatments. A multisurface dynamical study including explicitly the open-shell structure of the F atom has appeared recently in the literature:[65] excited *ab initio* PESs are included in the reaction dynamics, electronically non-adiabatic transitions are discussed and the different reactivity of the two F spin–orbit states is pointed out. However the conclusions of this work were that the reactivity of the $^2P_{1/2}$ state is a minor event with respect to that of the $^2P_{3/2}$, and thus, considering also the low fraction of $^2P_{1/2}$ contained in the beams, its contribution is often negligible. This explains why electronically adiabatic calculations can be accurate enough to reproduce most of the experimental measurements. Obviously, they must be amended when the dynamics at the threshold energies is investigated, as in the experiment of ref. 56 where very low energy beams are used to study the reactivity in rotational levels energetically closed to the $j = 3/2$ state. In this case electronically non-adiabatic effects arise, and can be explained only by a multi-surfaces formulation of the dynamics. In any case, from the comparison among SW,[25] HSW[48,57] and exact multi-surface calculation[65] and from ref. 66 for the D_2 case, it is possible to conclude that the electronically adiabatic dynamics is accurate when spin–orbit corrections are properly included to give the correct asymptotic correlation. It is clear that this permits only the study of the dynamics of the $^2P_{3/2}$ state.

In ref. 42 the spin–orbit operator ($\hat{H}_{so} = -\frac{2}{3}\,\delta\,\hat{\boldsymbol{L}}\cdot\hat{\boldsymbol{S}}$ has also been introduced and the complete matrix representation of $V + \hat{H}_{so}$ has been obtained on a spin-corrected basis set $|\Lambda\Sigma\rangle$, labeling the projections of the orbital and spin electronic angular momenta (see ref. 42 for more detail):

$$\boldsymbol{V} = \boldsymbol{A} + \mathrm{i}\boldsymbol{B} \tag{5}$$

where

$$\boldsymbol{A} = \begin{pmatrix} V_{00} + \frac{2}{5}V_{20} & 0 & \sqrt{2}/3\,\delta \\ 0 & V_{00} - \frac{1}{5}V_{20} - \delta/3 & -\frac{\sqrt{6}}{5}V_{22} \\ \sqrt{2}/3\,\delta & -\frac{\sqrt{6}}{5}V_{22} & V_{00} - \frac{1}{5}V_{20} - \delta/3 \end{pmatrix} \begin{matrix} |0\,1/2\rangle \\ |-1\,-1/2\rangle \\ |1\,-1/2\rangle \end{matrix} \tag{6}$$

and

$$\boldsymbol{B} = \begin{pmatrix} 0 & \frac{\sqrt{3}}{5}V_{21} & -\frac{\sqrt{3}}{5}V_{21} \\ -\frac{\sqrt{3}}{5}V_{21} & 0 & 0 \\ \frac{\sqrt{3}}{5}V_{21} & 0 & 0 \end{pmatrix} \begin{matrix} |\,0\ -1/2\rangle \\ |\,1\ 1/2\rangle \\ |\,-1\ 1/2\rangle \end{matrix} \tag{7}$$

where $V_{l_2\mu}$ have been defined in eqn. (4). In eqn. (6) the spin–orbit constant δ is taken independent of R and equal to the spin–orbit splitting of the open-shell atom, specifically 50.1 meV (1.16 kcal mol^{-1}). From the diagonalization of the Hermitian matrix (5), we obtain three surfaces, the ground one being merged with the SW PES (see below) and thus designated the SW-LR-SO surface because it is corrected for the spin–orbit interaction and shows the proper asymptotic correlation with the $^2P_{3/2}$ of fluorine. In this case, as well as for the diagonalization of the matrix (3) in Section II.A, the excited surfaces can also be obtained, but they will not be considered in this paper.

The aim of the present study is to evaluate the influence of the long-range forces and of the spin–orbit interaction on the reaction. To this purpose, we have to make explicit the fact that the two semi-empirical surfaces (SW-LR and SW-LR-SO) have a dependence on the bond length r of the H_2 molecule, and not only on the intermolecular distance R and on the bending angle θ, see Fig. 1 in ref. 42. The value of r was considered fixed at the equilibrium distance of 0.74 Å (this being justified by the fact that we take semi-empirical surfaces only in the entrance channel where the incoming atom just produces a small perturbation of the molecular states). In order to account for molecular rearrangement such as stretch and eventually the breaking of the H–H bond when reaction occurs, we had to join our representations with the complete SW surface which also permits the chemical reaction.

In order to accomplish this merging, two different problems must be solved. On the one hand, we have to introduce a dependence of our surface on the stretching H–H, *i.e.* on the variable r; on the other hand, our empirical surfaces must be joined with the reactive one when the intermolecular distance R decreases, leading to the transition state region and then to the products' valley.

As far as the r dependence is concerned, we constrain our surfaces to have exactly the dependence predicted from *ab initio* calculations by Stark and Werner. For each nuclear configuration, that is for each value of R, r and θ, the potential energy has been obtained by shifting the SW energies in such a

way as to make the value corresponding to the H_2 equilibrium distance coincident with that of our surfaces.

The merging procedure of our surfaces with the reactive one as R decreases is a slightly more complicated matter. We believe that our experimentally based characterization of the reactants' potential well, or more precisely of its negative area (see Fig. 2 in ref. 42), is more accurate than that provided by the SW fitting and then must be preserved. This region of the interaction determines the elastic and inelastic properties of the system and, indeed, from these measurements our surfaces have been derived. We leave unchanged the potentials in this region in order to preserve the reproducibility of the measured elastic and inelastic properties.

In doing such a merging, we have to take into account that the localization of the well along R is a function of the bending angle θ; more precisely, the position of the minimum and of the crossing with the zero of the potential (we specify that the latter is situated at infinite separation of the interacting partners F–H_2), shift at different R values as the bending angle varies (see Fig. 2). Therefore, for each θ value a spline cubic function has been used to join our surfaces to the SW one. The spline function starts at the R_0 value where our PESs cross the zero of the potential and reaches the SW PES for R displaced by one unit ($R_0 - 1$ Å). The use of spline cubic functions assures the continuity and the derivability of the global surface functions. The routine for the computation of the surfaces is available on request from the authors.

As a result of the described procedure, the SW-LR and SW-LR-SO surfaces have, in common with the theoretical SW surface, the saddle-point region and the exit channel of the reaction, while all differences are localized in the entrance channel.

In Fig. 2 (see also ref. 42), we can appreciate the differences in the well depths and in the positions of the minima between our surfaces and the SW one. For the perpendicular approach, the present treatment provides an interaction energy more attractive at long distances but much more repulsive when R decreases. In the intermediate region, the balance of the two components of the interaction produces a deeper well (about 0.45 kcal mol^{-1}) localized at a larger distance (2.7 Å). In the collinear geometry, the wells have similar depth (about 0.12 kcal mol^{-1} localized at 3.4 Å) but they look very different in the repulsive wall.

In Fig. 3, the angular dependence of the *ab initio* PES and of the modified versions SW-LR and SW-LR-SO on the orientation of H_2 is shown for a fixed value of the intermolecular distance R. The SW-LR and SW-LR-SO surfaces are found to be more anisotropic than the SW one, which appears flatter. An important role is in this case played by the V_{22}^4 coefficient, which describes the electrostatic interaction between the permanent quadrupole of the atom and of the molecule. The effects of this term are in this case (because of the Σ nature of the molecular orbital) repulsive for the linear geometry and attractive for the bent approach, giving a strong contribution to the description of the anisotropy of the interaction.

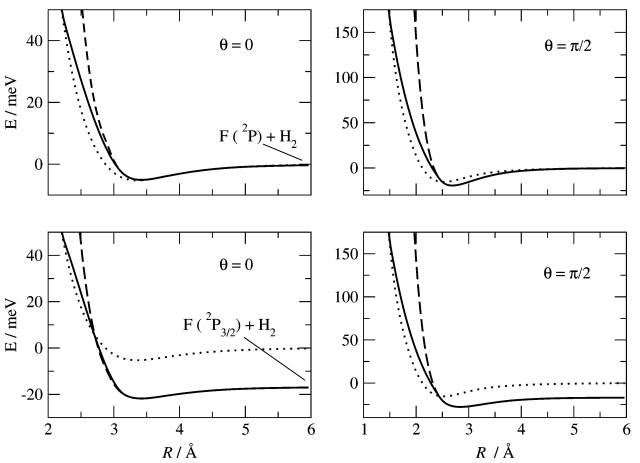

Fig. 2 Entrance channel for the SW-LR PES (solid line in the upper panels) and SW-LR-SO PES (solid line in lower panels) as a function of R for collinear ($\theta = 0$) and perpendicular ($\theta = \pi/2$) geometries. The intramolecular distance in H_2 is fixed at the equilibrium value, 0.74 Å. Note the asymptotic correlation for the SW-LR-SO PES with the $^2P_{3/2}$ state of the fluorine atom. In all panels, dotted curves correspond to the original SW surface, and dashed curves to the long-range potentials of ref. 42.

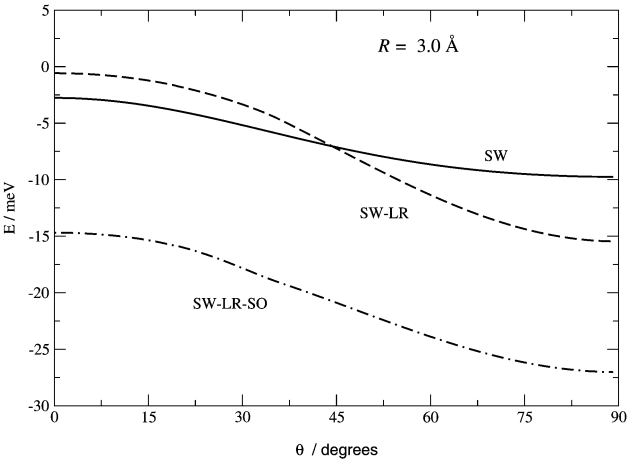

Fig. 3 Entrance channel for the SW (solid line), SW-LR (dashed line) and SW-LR-SO PESs (dashed-dotted line) as a function of the H_2 molecule orientation in the neighborhood of the van der Waals well. Angles $\theta = 0$ and 90° correspond to collinear and T-shape configurations, respectively. The intramolecular distance in H_2 is fixed at the equilibrium value, 0.74 Å.

Table 1 Comparison of the T-shape van der Waals minima of the ground F + H_2 PES. The distance H–H is kept fixed to the H_2 equilibrium distance, 0.74 Å

PES	R/Å	Well depths/kcal mol^{-1}
SW[a]	2.59	0.37
SW-LR	2.69	0.45
HSW[b]	2.85	0.18
SW-LR-SO	2.84	0.25

[a] Ref. 20. [b] Ref. 48.

The depths and the geometries of the van der Waals minima are compared in Table 1 for our two modified surfaces, for the original SW and for the spin-corrected HSW. The effects of the spin–orbit interaction on the van der Waals geometries are essentially to pull the well at larger R value and to halve the depth. We can notice that the same effects on the minima of the wells are given for the HSW corrections for which the geometry of the minimum is very similar to the SW-LR-SO PES. However different anisotropy of the correction was used in the HSW PES because the spin–orbit correction had been assumed independent of the Jacobi angle θ. In Section IV we shall discuss changes in dynamical quantities (integral and differential cross sections) due to the proposed modifications of the entrance channel.

III. The hyperquantization algorithm

For the solution of the dynamical problem, we use a time-independent hyperspherical approach adopting an adiabatic representation with respect to the hyperradius ρ. The ρ range is

discretized on a grid and the dynamical problem is separated in two different steps. First, an eigenvalue problem is solved at the selected values of the hyperradius, and the outcome of this step is effective hyperspherical potentials (or adiabatic curves) upon which the reaction evolves. In the second step, the hyperradial solutions are propagated from small to large ρ values, corresponding respectively to the strong triatomic interaction region, and the asymptotic separation of reactants or products.

We have developed an original method for the solution of the ρ-fixed eigenvalue problem. The method is called hyperquantization algorithm and has been presented in a number of papers,[44,45,67] to which we refer for its theoretical introduction. Here, only some general features will be outlined.

The ρ-fixed eigenvalue problem to obtain effective hyperspherical eigenvalues is the key-step in the hyperspherical approach to reaction dynamics, and the quality of the results which are obtained is strongly dependent on the accuracy in solving this equation, *i.e.* in calculating the adiabatic eigenvalues, the corresponding eigenvectors and all the quantities related to them (rotational and Coriolis coupling matrix elements and overlap between sectors). In this application of the hyperquantization algorithm we use the symmetric hyperangular parametrization of the hyperspherical coordinates in the inertia principal axis frame. Alternatives have been considered elsewhere.[67] Basic tools of the algorithm are Hahn polynomials[68] (generalizations of 3-*j* symbols), used as discrete analogs of hyperspherical harmonics. Exploiting the mathematical property of these polynomials, the matrix representation of the Hamiltonian is very sparse and highly symmetric. These features are most valuable from a computational point of view, as is the fact that the algorithm does not require the calculation of any numerical integral. Diagonalization of very sparse large matrices can be performed very efficiently by Lanczos diagonalization techniques.[67]

In the proposed "stereodirected" representation, the domain of the internal angular variables Θ and Φ is discretized on a grid of points labeled by the indices τ and v, respectively (see eqn. (38) and (40) in ref. 45). The first parameters to be specified are the number of lattice points, I and N, for the discretization of the angular variables. Provided that the labels τ and v are the Hamiltonian matrix indices, the values of I and N are critical for the effectiveness of the method, being directly related to the matrix dimension. Because of the particular kind of discretization proper of the hyperquantization algorithm, a very large number of points is needed to accurately represent the space of the Θ variable, while a much smaller number is necessary for Φ. Obviously, optimal choices for both I and N are functions of the hyperradius ρ, the reaction coordinate in the hyperspherical representation (see Table 2), and are strongly dependent on the topology of the employed potential energy surface (a more detailed discussion is given in ref. 67).

Table 2 Numerical parameters for the production runs of the hyperquantization algorithm code

ρ/a_0	I	N	V_{max}/eV	e_{cut}/eV	n_{cut}
Truncation on Θ_τ					
12	11 800	272	3.5	6.5	15
11	10 800	248	3.5	6.5	15
10	9400	224	3.5	6.5	15
9	8000	200	3.5	6.5	15
8	7000	180	3.5	7.2	16
7	6000	156	3.5	7.5	18
6	4500	136	3.4	10.0	22
5	2800	112	3.2	53.0	42
Truncation on Φ_v					
4	1500	100			34
3	1500	100			23
2.2	1500	100			19

Each τ and v pair individuates a particular configuration of the triatomic system at a given ρ. Points where the potential value is very high (in general larger than a threshold value V_{max} determined by numerical convergence on the eigenvalues of eqn. (41) in ref. 45) are expected to give a negligible contribution to the total eigenfunction: the amplitude of the eigenvectors in these points will be very small. Because of it, these τ and v pairs can be eliminated, leading to a substantial reduction in the Hamiltonian matrix dimension and strongly increasing the efficiency of our approach. The size of this cut-off depends also on ρ (see also ref. 67).

The parameters n_{cut} and e_{cut} of the diagonalization-truncation procedure which we apply to our algorithm (see ref. 69) must also be determined. They define the number of states n_{cut} to be retained for each block of the Hamiltonian matrix in the first diagonalization step, requiring proper coverage of the channels relevant up to a given maximum energy e_{cut}. As for the V_{max} parameter, their values are established by numerical convergence on the eigenvalues.

Numerical values of all discussed parameters used in the "production runs" are shown in Table 2 as a function of the reaction coordinate ρ. The convergence criterium used is very strict and therefore the values of Table 2 are largely overestimated (see ref. 69 for a less demanding computer time choice). This choice ensures that all the open adiabatic eigenvalues of the reaction are converged within a few tenths of a meV and this leads to integral cross sections converged within less than 0.01 Å^2. This convergence level is stricter than normally required and has been chosen to focus attention on the accuracy and the reliability of the calculational technique rather than to optimize the computer performance of our algorithm.

The ρ-fixed eigenvalue problem (eqn. (41) in ref. 45) solved by the hyperquantization algorithm depends parametrically on the projection Ω of the total angular momentum J along the minimum inertia axis (that is the quantization axis of the chosen rotating frame). An eigenvalue problem must be solved for each Ω value. However, it does not depend on the value of the total J, because of the adopted partition of the total Hamiltonian (see eqn. (14) in ref. 45 and related discussion). The residual matrix (W in ref. 45) depends explicitly on the J values, its elements couple the eigenstates belonging to different Ω, and is handled in the propagation step. In general, not all the allowed projections must be retained, and the fact that their number can be truncated leads to an enormous reduction in the number of the eigenstates to be propagated.

In the present case, we include values up to 5 for Ω, and up to 25 for J. Actually $\Omega_{max} = 3$ is large enough to give converged integral cross sections but this value must increase up to 5 to eliminate all spurious oscillations in the differential cross sections. These values are in agreement with other computational papers based on different theoretical approaches.[7,25,48] The number of closed channels included in the calculations are the same as in ref. 7: for $\Omega = 0$, we have calculated 150 adiabatic eigenstates and for the subsequent Ω values, this number decreases according to the number of permitted asymptotic states. The total number of coupled channel is 784 for $J \geqslant 5$. Some tests of the convergence of this choice have lead to a maximum uncertainty of 0.03 Å^2 in the integral cross sections (this can be considered the global truncation basis error of our calculations).

The computer code is therefore organized as follow: a first run using the hyperquantization algorithm performs the calculation of the Ω-dependent basis set and the coupling between them (the residual matrix W). This is the heart of the calculation and is normally the most demanding part of the code in terms of computer memory. Exploiting the diagonalization truncation technique, N tridiagonal matrices of dimension I

are diagonalized and the first n_{cut} eigenvectors of energy less than e_{cut}, are coupled by the off-diagonal kinetic elements, to give a full matrix of maximum dimension $(\frac{N}{2}+1)\times n_{cut}$ (however the effective order of the matrix is much lower, especially at large ρ, as a consequence of the effect of the reduction parameters e_{cut} and V_{max}). Diagonalization of this matrix gives the required eigenvalues while the eigenvectors are given by the product of the preceding $(\frac{N}{2}+1)\times n_{cut}$ eigenvectors times the eigenvectors of the final matrix. Eigenvectors in factorized form are used directly to give efficiently the overlap between the hyperradial sectors. When a change of grid is required the unfactorized eigenvectors are numerically interpolated to project on the new grid. At small values of ρ an alternative diagonalization-truncation scheme is more efficient and $I+1$ full matrices of dimension $\frac{N}{2}+1$ are diagonalized. The resulting final matrix (obtained by coupling the first n_{cut} eigenvectors of each block) is block-tridiagonal and is efficiently diagonalized by the spectral transform Lanczos method.[70]

Once the adiabatic states are generated and stored, they can be used as input file for running the number of partial waves and collision energies required with another computer code. The advantage of dividing the program into two parts is that, once generated, the adiabatic states can be used for different collision energy ranges by simply changing in the second step, the values of the energies and the number of partial waves. Adiabatic hyperspherical curves have been propagated from $\rho = 2.2\ a_0$ till the asymptotic limit of $\rho = 12\ a_0$, along 50 ρ sectors. The Johnson log-derivative technique[71] modified by Manolopoulos[72] has been used.

When wide range or a very fine grid in the collision energies is required to study for instance resonance structures, this part of the code can become the most demanding in terms of computer time. However, since the propagation of each partial wave is an independent calculation and since the propagation itself is an essentially sequential procedure (and therefore cheap from the memory point of view), this part of the code can be very efficiently parallelized. This reduction of computer times can be very important when a large number of channels must be propagated as needed for extensions to systems where all three atoms are different. In this work a parallel version of this part of the code has been used.

IV. Results

Dynamical calculations by the hyperquantization algorithm code have been performed for the $F + H_2$ reaction using first the original SW surface[20] and then our surfaces modified for the long-range interaction (SW-LR) and for the spin–orbit effect (SW-LR-SO), see Section II.

We performed the calculations at six different collision energies for the purpose of direct comparison with the experimental results. Integral and differential cross sections have been calculated for both para-hydrogen (rotational states $j = 0$ and 2) and ortho-hydrogen ($j = 1$ and 3), and for the ground H_2 $v = 0$ vibrational state. Reactive scattering calculations for $j = 3$ are presented for the first time in this work.

The outcome of our procedure is the extraction of the S-matrix, whose elements $S^J_{vjK,\ v'j'K'}$ are directly related to the probability to obtain the final rovibrational state v', j' of the products' arrangement channel starting from the rovibrational state v, j in the reactants' arrangement channel; K is the quantum number of the projection of the total angular momentum quantum number along the Jacobi vector length R for the corresponding asymptotic channel. State-to-state differential and integral cross sections can be directly extracted from an appropriate linear combination of the calculated parity adapted S-matrix elements in the center-of-mass frame. The partial wave expansion for the differential cross sections in the helicity representation is:

$$\sigma_{vjK,\ v'j'K'}(\vartheta_{CM}) = \frac{1}{4k^2_{vj}}\left|\sum_J (2J+1) d^J_{K,K'}[\cos(\pi - \vartheta_{CM})] S^J_{vjK,\ v'j'K'}\right|^2 \quad (8)$$

where ϑ_{CM} is the angle between the incident relative F velocity vector and outgoing relative HF velocity vector. The $d^J_{K,K'}$ in eqn. (8) are reduced Wigner d functions and k_{vj} is the initial wavenumber. The integral cross sections are obtained as follows:

$$Q_{vjK,\ v'j'K'}(E) = \frac{\pi}{k^2_{vj}} \sum_J (2J+1)|S^J_{vjK,\ v'j'K'}|^2 \quad (9)$$

The quantities in eqn. (8) and (9), appropriately summed and averaged according to experimental conditions, are those to be compared with the experimental data.

The comparison of our results (state-to-state reactive integral and differential cross sections on the SW, SW-LR and SW-LR-SO PESs) with experiments allows us to interpret all differences in the dynamical quantities calculated on our modified surfaces in terms of the description of the potential well and of the asymptotic behavior in the entrance channel. In this way, the effects of a more accurate characterization of the long-range potential well and of the introduction of the spin–orbit effect on the dynamics can be singled out.

Differential and state-to-state integral cross sections, at the three collision energies 1.84, 2.74 and 3.42 kcal mol^{-1} for rotational angular momentum of the reactant hydrogen molecule $j = 0$, 1, 2 have been compared with the calculations of ref. 48 on the same potential energy surface, in order to test the reliability and the accuracy of the hyperquantization algorithm code. The level of agreement between the two different calculations is very good and differences cannot be appreciated at the level of the scale of the figures of this paper. However a detailed comparison of the numerical values of the

Table 3 Product rotational summed integral cross sections for the $F + H_2\ (j) \rightarrow HF(v') + H$ reaction in $Å^2$ on the SW PES

	Collision energy/kcal mol^-					
	1.84		2.74		3.42	
v'	This work	ref. 48[a]	This work	ref. 48[a]	This work	ref. 48[a]
$j=0$						
0	0.03	0.04	0.08	0.08	0.13	0.13
1	0.63	0.63	1.18	1.21	1.56	1.59
2	3.42	3.50	4.58	4.63	4.67	4.69
3	1.43	1.36	0.90	0.82	0.74	0.67
All	5.52	5.53	6.74	6.74	7.10	7.08
$j=1$						
0	0.03	0.03	0.08	0.08	0.12	0.13
1	0.54	0.55	1.07	1.08	1.40	1.42
2	3.39	3.49	4.08	4.15	4.34	4.37
3	1.73	1.63	1.86	1.78	1.74	1.67
All	5.68	5.70	7.08	7.10	7.60	7.59
$j=2$						
0	0.04	0.04	0.08	0.09	0.12	0.13
1	0.75	0.75	1.11	1.11	1.37	1.36
2	3.19	3.31	3.82	3.90	4.02	4.10
3	2.01	1.92	2.42	2.35	2.46	2.38
All	5.99	6.02	7.43	7.44	7.97	7.97
$j=3$						
0			0.13		0.17	
1			1.39		1.57	
2			3.66		3.81	
3			2.58		2.69	
All			7.76		8.24	

[a] Minor corrections were kindly pointed out by J. F. Castillo.

integral cross sections (see Table 3) show some minor differences. Integral cross sections (summed on the rotational angular momentum of the products) differ in some cases by about 0.1 Å^2 for the third vibrational level (this is outside our truncation basis error estimate given in section III) so that we find "hotter" vibrational distributions than those of ref. 48, in agreement with the experimental trend[3] (see Section IVB). These minor discrepancies tend to disappear for total cross sections (summed also on the vibrational states of the products). This effect has been observed at all the energies and initial rotational angular momentum studied and the discrepancy on the $v'=3$ vibrational branching ratios range from 0.05 (for $E_{coll}=1.84$ kcal mol^{-1}) to 0.03 for the other two energies. No differences have been found for $v'=0$ and 1 where the previously published vibrational branching ratios have been satisfactorily reproduced.

In order to investigate the nature of these small differences some of the calculations have been repeated using the code of ref. 7, obtaining close agreement with our results (within 0.01 Å^2), even though our code and that of ref. 7 cannot be considered totally independent: the same hyperspherical coordinates (symmetric representation, see Section III) and the same propagation scheme are used, while ref. 48 adopts a hyperspherical asymmetric overcomplete channel representation.

All these comparisons serve to establish the reliability of the hyperquantization algorithm and its full capability of yielding converged differential and integral cross sections for triatomic reactions.

A. Differential cross sections

To compare calculated and experimental differential cross sections (DCS) we have simulated the reactants rotational distributions of the beam of ref. 3 as in Table 1 of ref. 27 and reported in Table 4 to simplify the reading of the paper. To obtain integral and differential cross sections for normal and para-hydrogen we sum over all rotational components after multiplying the cross sections for each initial rotational state of the reactants by the appropriate relative rotational population.

Fig. 4 shows calculated differential cross sections, summed over the rotational product quantum states, for the reaction F + p-H_2 → HF (v) + H at the lowest of the three investigated collision energies. In Fig. 5, the case of F + n-H_2 → HF + H reaction is shown, again at collision energy of 1.84 kcal mol^{-1}. In both figures the different curves represent different final vibrational states of the HF molecule (the $v'=0$ case is not appreciable on the scale of the figures at this collision energy). Comparison is shown between results on the SW potential energy surface, those obtained on the new SW-LR-SO and the experiments. Vibrationally summed differential cross sections are also reported. Analogous pictures for normal hydrogen for the other two considered collision energies (2.74 and 3.42 kcal mol^{-1}) are shown in Fig. 6 and Fig. 7, respectively.

Table 4 Estimated rotational temperatures, T_{rot} and relative populations, of the H_2 in the beam experiment of ref. 3

Reactants	E_{coll}/ kcal mol^{-1}	T_{rot}/K	$j=0$	$j=1$	$j=2$	$j=3$
F + p-H_2	1.84	170	0.80	0.00	0.20	0.00
F + n-H_2	1.84	170	0.20	0.74	0.05	0.01
F + n-H_2	2.74	260	0.15	0.69	0.10	0.06
F + n-H_2	3.42	325	0.12	0.64	0.12	0.12

From the analysis of these figures we can notice that the qualitative shape of DCS does not vary for the new surface, even though a clear improvement of the agreement between experiments and theory with the spin–orbit corrected surface is shown. In particular the forward peak is lower at all the energies although less so as the collision energy increases. The best improvement is obtained for normal hydrogen at 1.84 kcal mol^{-1}, being the ratio between backward and forward scattering for the v' summed DCS about three, in excellent agreement with experimental results. For the SW surface this ratio is ~ 1.5.

For the other two energies the experimental forward peak is smaller than calculated even when the long-range corrections are introduced, and no $v'=2$ forward products have been observed. However, no error bars were given for the experimental data[3] and as has been stressed elsewhere,[25] the HF ($v'=2$) product scattered in the forward direction was partially obscured by the F atom reactant beam because of the kinematics of the molecular beam experiment. The cross section for $v'=2$ in the forward direction should be small and it is possible that even if some $v'=2$ vibrationally excited product had been present, it would have been too difficult to detect.

The most prominent effect of spin–orbit correction in the differential cross section calculations is the decrease of the forward–backward peak ratios. It is known (see also ref. 25) that the forward peak is due to high partial waves, which in classical mechanics correspond to trajectories with large impact parameters. Indeed, the spin–orbit correction (see in Fig. 3) decreases the van der Waals well of the reactants and changes the anisotropy of the potential at long-range, affecting high partial waves and therefore the forward peak. This effect, as confirmed from the numerical results, is more important at lower collision energies. It is interesting to remark that a similar role of the spin–orbit correction had been found in ref. 48, using the HSW surface.

As outlined in the Introduction, two alternative mechanisms have been proposed in the literature as responsible for forward scattering: one is direct tunneling through the centrifugal barrier and the other is a shape resonance feature which binds the system. Ref. 25 dedicates much effort to discriminating between these mechanisms. The conclusion was in favor of the direct mechanism, although a contribution from quantum resonances in the product channel cannot be ruled out.

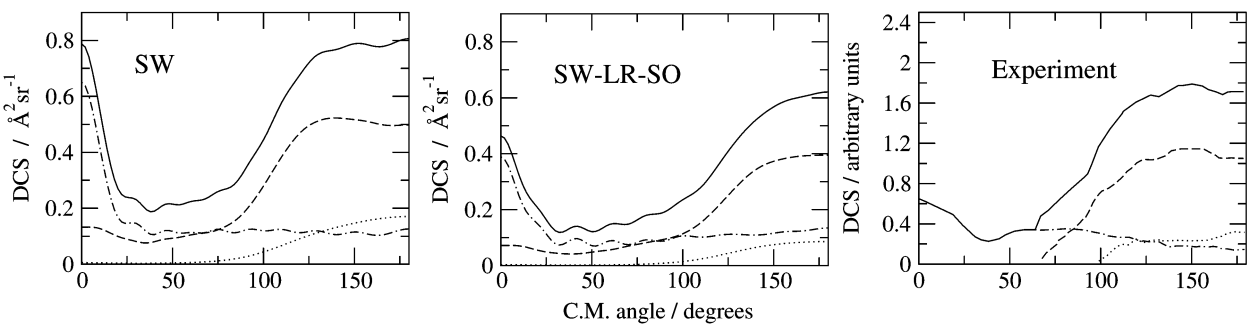

Fig. 4 Differential cross sections for the reaction of para-hydrogen summed over the rotational states j' of the products calculated for the SW and for the SW-LR-SO PES. The collision energy is 1.84 kcal mol^{-1}. The last panel shows the experimental results by Neumark and co-workers.[3] Dotted, dashed and dash-dotted curves are for product vibrational states of HF $v'=1$, 2 and 3, respectively. Solid curves are their sum.

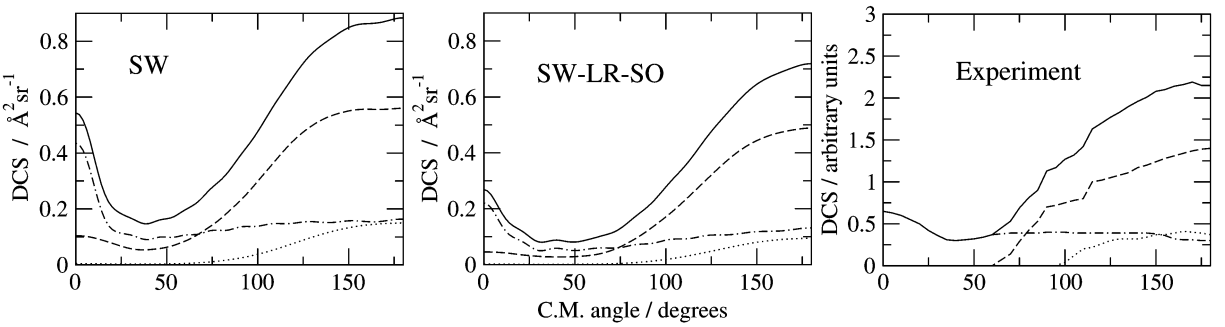

Fig. 5 As in Fig. 4 for the reaction of normal-hydrogen at the collision energy 1.84 kcal mol^{-1}.

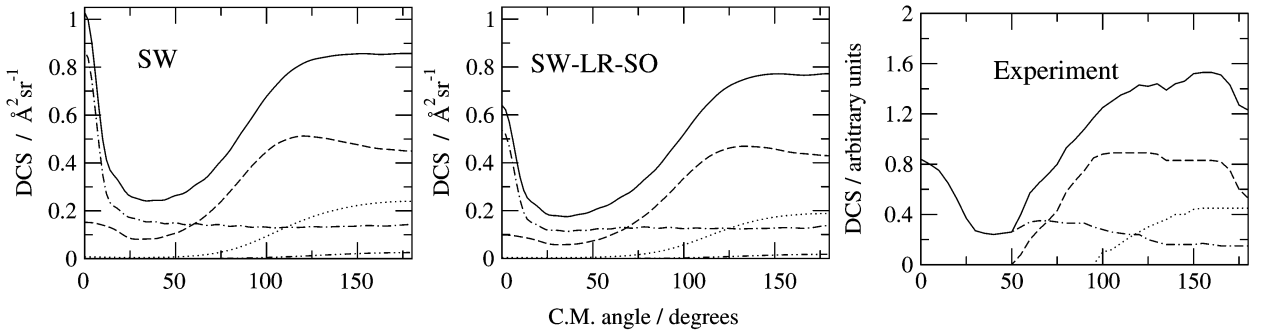

Fig. 6 As in Fig. 4 for the reaction of normal-hydrogen at the collision energy 2.74 kcal mol^{-1}. The $v' = 0$ curve is also shown.

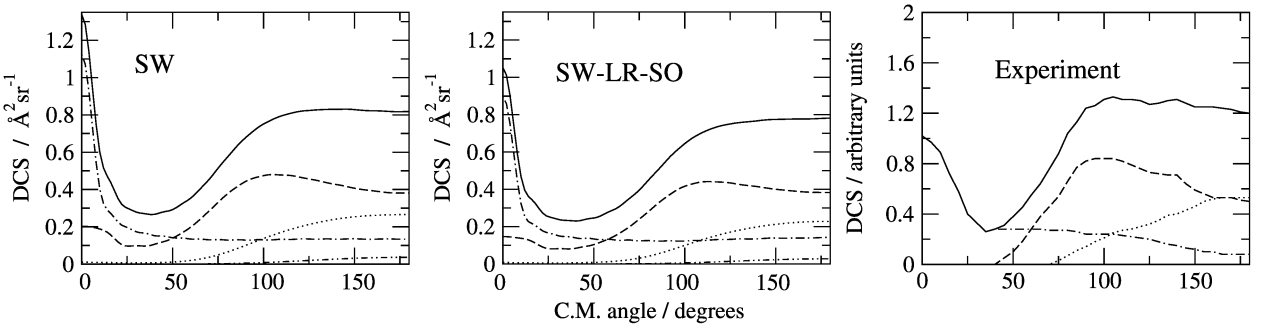

Fig. 7 As in Fig. 6 for the reaction of normal-hydrogen at the collision energy 3.42 kcal mol^{-1}.

We remark that our results are consistent with both mechanisms. In fact we can imagine that the resonance contribution can be washed out because of the decreasing in the van der Waals well depth, moving out or eventually deleting quasi-bound states supporting the resonance. From the other point of view we notice that another effect of the spin–orbit corrections is to increase the barrier of the reaction. This increase disfavors reactivity, in particular preventing tunneling which depends exponentially on the height of the barrier. But even though we cannot support either of the two mechanisms we can say, at variance with the conclusions of ref. 25, that if the forward peak decreases because of a resonance, this must be localized in the entrance channel which is the only feature modified in our surface.

Similar calculations have been performed also with our SW-LR PES modified only in the van der Waals region with no spin–orbit correction (see Section II.A). The results indicate that the differential cross sections for an initial rotational state larger than zero are essentially the same as for the SW PES and small deviations for the ground rotational state of hydrogen are washed out, averaging on the rotational temperature. This aspect appears to support the direct mechanism, even though it might also be true that the modifications adopted are simply too small to be detected in this range of collision energies.

In conclusion, we observe that the proposed spin–orbit correction improves the agreement with the experimental forward–backward cross section ratios at all the investigated energies, while the effect of the van der Waals corrections is negligible for this quantity.

B. Vibrational branching ratios

Table 5 shows vibrational branching ratios with respect to HF ($v' = 2$). Experimental branching ratios (as measured in two different experiments[3,36]) are compared with calculations on both the SW surface and on the long-range modified spin–orbit surface SW-LR-SO, and with the results of Castillo *et al.*[48] on the HSW surface. Ratios are presented between integral cross sections rotationally summed for each vibrational state of the products with respect to $v' = 2$, which is the most populated product channel. Error bars are our estimates propagating uncertainties in populations as given in ref. 36.

Integral cross sections have been averaged over the reactants rotational states to cope with different experimental beam

Table 5 Comparison of experimental branching ratios (ref. 3 for the $F + p\text{-}H_2$ reaction and both ref. 3 and 36 for the $F + n\text{-}H_2$ reaction) with quantum calculations on the SW, HSW (ref. 48), SW-LR-SO surfaces

v'	SW	HSW	SW-LR-SO	Experiments
$F + p\text{-}H_2$				
$E_{coll} = 1.84$ kcal mol^{-1}				
0	0.01		0.01	
1	0.19	0.15	0.15	0.20
3	0.46	0.50	0.69	0.68
$F + n\text{-}H_2$				
$E_{coll} = 1.84$ kcal mol^{-1}				
0	0.01		0.01	
1	0.17	0.14	0.14	0.21
3	0.50	0.39	0.47	0.67
$E_{coll} = 2.4 \pm 0.6$ kcal mol^{-1}				
0	0.02 (0.01–0.02)		0.01 (0.01–0.02)	< 0.04
1	0.23 (0.16–0.28)		0.18 (0.13–0.24)	0.35 ± 0.07
3	0.42 (0.49–0.36)		0.49 (0.47–0.42)	0.50 ± 0.03
$E_{coll} = 2.74$ kcal mol^{-1}				
0	0.02	0.01	0.01	
1	0.27	0.22	0.23	0.23
3	0.44	0.42	0.48	0.53
$E_{coll} = 3.42$ kcal mol^{-1}				
0	0.03	0.02	0.02	
1	0.33	0.29	0.30	0.33
3	0.43	0.40	0.46	0.48

conditions: as for the differential cross sections, the coefficients of Table 4 have been used for the simulation of the beam of ref. 3 while statistical weights ($j = 1$ and $j = 0$ in the ratio of 3 : 1) have been taken in order to compare with the experiment of ref. 36, where very low rotational temperatures are reached in the supersonic expansion. Actually $j = 3$ cross sections had not been calculated in ref. 48 but we have checked that the approximation made in that paper, neglecting the difference between $j = 3$ and $j = 2$ cross sections, is quantitatively accurate, so that the HSW and SW-LR-SO results can be consistently compared.

Despite the high rotational resolution in the reactive beam and in the product detection, the velocity spread in the Chapman *et al.*'s[36] beam is very large, so that the results of the calculations should be averaged on the collision energy distribution (not given in that work). Comparison with that experiment has been done by calculating the integral cross sections at the most probable collision energy (2.4 kcal mol^{-1}) and at the extremes of the confidence range (1.8 and 3.0 kcal mol^{-1}). As can be seen from Table 5, variations of $v' = 3$ branching ratio within the energy uncertainty range are larger than the error bars of the experiment and cannot be neglected.

The comparison between SW and SW-LR-SO values shows that inclusion of spin–orbit in the $v' = 1$ vibrational level in all considered cases results in a decrease in the ratio (even if within the experimental error bars). A perfect agreement is found with the branching ratios of the HSW calculations at all the investigated energies, and this concordance can be attributed to the increase of the reaction barrier height which is a common feature between the HSW and SW-LR-SO potential energy surfaces.

This decrease in the $v' = 1$ ratios spoils (except for the intermediate energy) the excellent agreement found with the SW PES for this quantity. However the differences found between the ratios calculated with the two surfaces, are of the same order of magnitude as the error bars of the experiments. Moreover the two experiments do not appear to agree regarding these ratios, those of ref. 3 being outside the large error bars of ref. 36.

For the $v' = 3$ case, for which the two experiments agree, the SW-LR-SO PES provide a better overall agreement than obtained with other surfaces, even when comparison is made with the HSW results.[48] This suggests that the agreement is not simply due to an increase in the reaction barrier.

As has been discussed in Section II, the largest difference between the HSW and our SW-LR-SO PESs is their anisotropy in the entrance channel (see Fig. 2), the angular dependence of the spin–orbit correction having been neglected for the HSW PES. Calculations using the SW-LR PES (not reported) show the sensitivity of the cross section ratios to the long-range corrections. In particular van der Waals effects are important for the para-hydrogen case: the value of 0.53 obtained for the $v' = 3$ branching ratio is an indication of a substantial contribution of the long-range forces to improve the agreement with experiments.

One possible explanation of the sensitivity of the $v' = 3$ cross sections to the anisotropy of the PES can be found in classical mechanical terms from the competition between the two saddle points of the reaction. Higher anisotropy can force the reactants to cross the transition state in a bent configuration, leading to vibrationally excited products (say, $v' = 3$) subtracting flux from trajectories which would have been going to react by a collinear approach. Collinearly dominated trajectories imply lower vibrational excitation. Increasing the rotational excitation of the reactants or the kinetic energy of the incoming atom, anisotropies become less influential and this effect dies off sharply. Therefore only for the para-hydrogen reaction (where 80% of reactant molecules are in their ground rotational state), is this effect relevant for the accurate description of the reaction dynamics. A similar effect of the van der Waals anisotropy has been recently discussed in terms of classical trajectories, regarding the inefficiency of rotational reactants excitations in the $Cl + H_2$ reaction.[73]

Moreover the spin–orbit correction pulls the van der Waals well at larger values of R, modifying the reaction probabilities for high partial waves (corresponding to large impact parameters). High angular momenta are very important for the production of the vibrational state $v' = 3$ and this explains the selective sensitivity of integral cross sections.

A better check of the anisotropy of the potential can be made by performing inelastic rotational cross section calculations, where very accurate measurements permit a detailed comparison with theory. Also the analysis of the stereodirected representation of the S matrix (for definitions and recipes see ref. 74–77), should give further insight on the study of the competition between different geometrical approaches to the reaction barrier.

C. Nascent rovibrational distributions

In Fig. 8 and 9 nascent rovibrational distributions are plotted as a function of the product rotational states for the open vibrational channels of the reaction and compared with the experimental data of Chapman and co-workers,[36] both for the SW surface and for the SW-LR-SO PES. In that experiment, as discussed in the preceding section, the reactant beam contained only ground states of ortho- and para-hydrogen statistically weighted (3 : 1).

As shown in the figures, almost no difference between the two surfaces has been found in the rotational distributions for the first two vibrational states. From both the calculations, symmetric distributions with respect to the most populated rotational states are found for practically all the collision energies investigated. The rotational distributions of the experiments are less symmetric and slightly colder. The $v' = 1$ vibrational state seems to have some structure which was not present in any calculations. However, except for some values of j', the overall accord is satisfactory, and most of the calculated values are within the experimental error bars. The

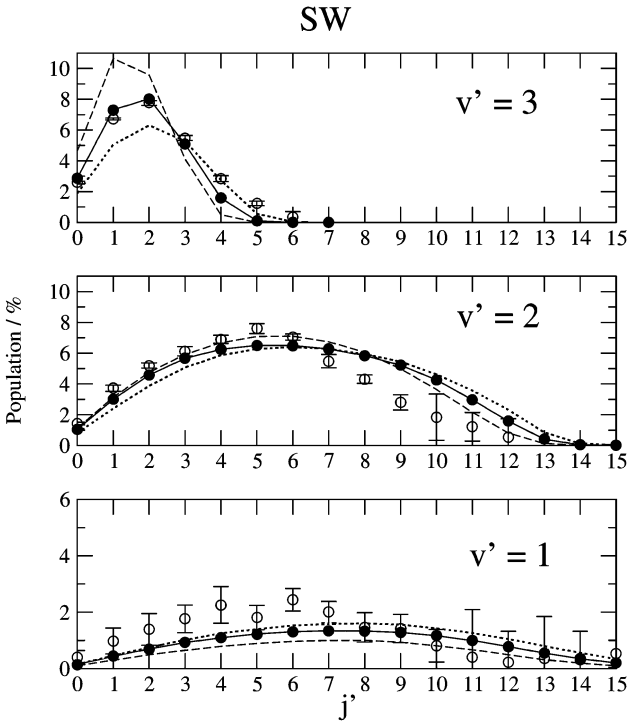

Fig. 8 Product rovibrational distributions for the SW surface. Full circles joined by solid curves are the theoretical calculations for the most probable collision energy of 2.4 kcal mol^{-1}, while dashed lines refer to the collision energies of 1.8 and 3.0 kcal mol^{-1} (lower and upper limit of uncertainty of the energy range of the experiment[36]). Empty circles with error bars are the experimental values.

agreement between the experimental and the theoretical distribution reflects the one found between the vibrational branching ratio (see Table 5). Again, a more interesting situation arises by $v' = 3$. Experiments show a rotational distribution peak at $j' = 2$ which dies at $j' = 6$. For the most probable collision energy, the calculation on the SW surface reproduces the position of the maximum, while for the spin–orbit corrected surface the integral cross section for $j' = 1$ is very similar to that for $j' = 2$. In all cases, computed distributions die before the experimental one and the integral cross sections become zero for the $j' = 5$ level, for which, experimentally, a not-negligible reactivity is found. As we have stressed in the Introduction section, this is due to the inaccuracy of the exoergicity of the SW PES.[78,79] If we account for the effect of the collision energy uncertainty, the shape of the distributions changes significantly. In fact, the calculated maximum shifts in all cases from $j' = 1$ to $j' = 2$ as the collision energy ranges from the lowest to the highest experimentally permitted values. Hotter rotational distributions are found increasing the collision energy. So even though the shape corresponding to the most probable collision energy is more closely reproduced by the original SW surface, the experimental spread makes it impossible to discriminate which one of the two calculations achieves a better agreement. Since the maximum of the distribution is very difficult to detect experimentally (it is very sensitive to the rotational energy of the reactants and hotter distributions are obtained as the initial j increases), it is likely that the presence of a small fraction of rotational states higher than $j = 1$ in the beam shifts the distribution significantly.

D. Total integral cross sections

In Fig. 10(a) and (b) another set of experiments and related calculations are compared with the present results. All the adiabatic calculations are divided by a factor of two to take into account the asymptotic degeneracy of the doublet surfaces. In panel (a), measured total integral cross sections as obtained by Dong and co-workers[31] are compared with the calculations on the SW surface and with our spin–orbit corrected SW-LR-SO PES. Para- and normal-hydrogen beams are simulated by mixing $j = 0$, 1 and 2 integral cross sections at $T_{rot} = 150$ K (which correspond to a population of about 13% for the first para-hydrogen excited rotational state $j = 2$.

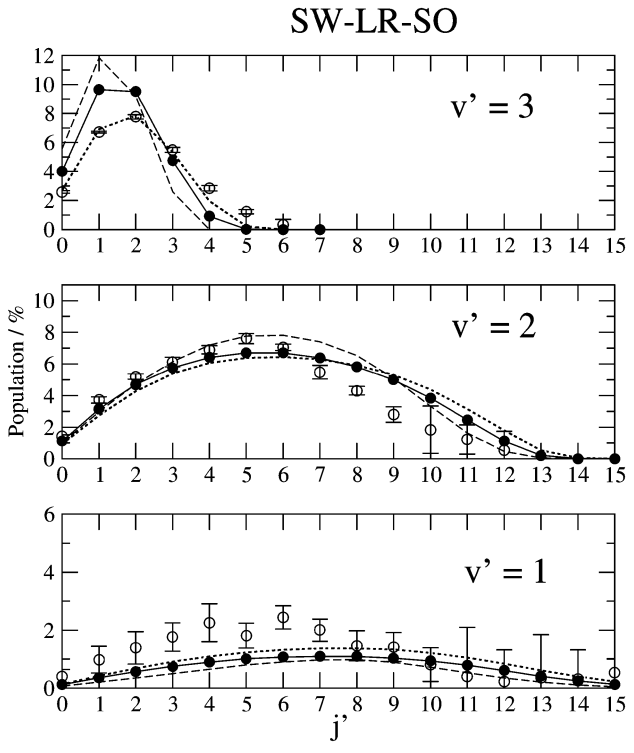

Fig. 9 As in Fig. 8 for the SW-LR-SO PES.

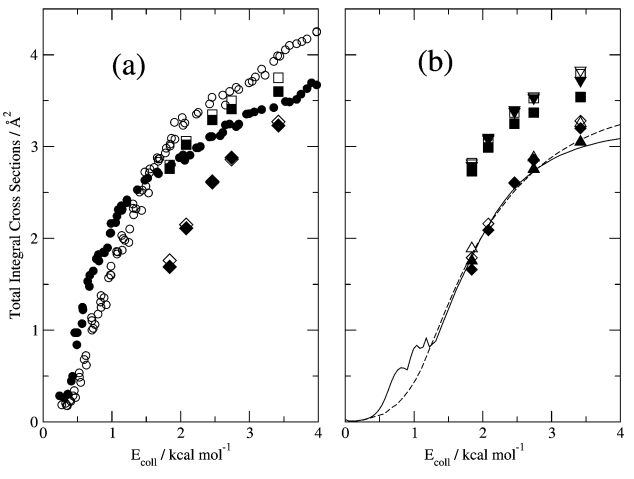

Fig. 10 Total integral cross sections as a function of the collision energy for the reaction $F + H_2 \rightarrow HF + H$. In the panel (a) para (full symbols) and normal (empty symbols) hydrogen simulations at $T_{rot} = 150$ K for the SW surface (squares) and for the SW-LR-SO (diamonds) are compared with the experimental results of ref. 31 (circles). In the panel (b) calculations of state selective rotational states of the reactants (empty and full symbols refer to $j = 0$ and 1, respectively) are compared: curves refer to the multisurface calculations of ref. 65 (solid and dashed for $j = 0$ and 1, respectively), triangles up refer to the HSW calculations of ref. 48, squares, triangles down and diamonds refer to the present calculations on the SW, SW-LR and SW-LR-SO PESs, respectively.

Contributions of higher j are less than 1% and will not be taken into account).

The comparison shows that the introduction of the long-range and spin–orbit corrections spoils significantly the good agreement of the original Stark–Werner surface. Indeed, total integral cross sections for the corrected surface drop to zero faster with collision energy than both the SW and the experimental results. At 1.84 kcal mol^{-1} they are already about one half of the experimental values. Both calculations tend to converge at higher collision energies. The effects of the rotational energy of the reactants (the ratio between para- and normal-hydrogen) is also clearly better simulated by the uncorrected surface, the SW-LR-SO results being fairly insensitive to the rotational excitation of the reactants. It should be noticed that the experiment does not provide the absolute values of cross sections,[31] but no energy independent scale factor can match the SW-LR-SO PES results: accordingly, the original scaling of ref. 31 (optimized on the F + HD total integral cross sections calculations performed on the SW surface) is adopted in the figure.

In panel (b), total integral cross sections at fixed values of initial j are plotted for $j=0$ and 1 for the three potential energy surfaces used in this work (SW, SW-LR, SW-LR-SO) and compared with ref. 48 and 65 (only the integral cross sections relative to the $^2P_{3/2}$ spin–orbit state of the fluorine atom, which are of interest here, are reported).

A surprisingly good agreement can be seen between our SW-LR-SO results and the calculations of ref. 48 and 65 which take into account the spin–orbit structure of the fluorine. This is a clear demonstration that the introduction of the spin–orbit correction in the adiabatic approximation frame is an excellent approximation for this system. Only small differences between fully coupled[65] and spin–orbit corrected surfaces can be seen at higher collision energies, but it is not clear if they are due to the different dynamical treatments or to the alternative fitting for the ground potential energy surface used in ref. 65.

From the comparison between our SW-LR-SO and SW-LR results we can notice that they are much more similar for $j=1$ and 2 (the $j=2$ case is not shown in order to not overcrowd the figure) than for $j=0$. The effect of the van der Waals corrections is therefore only to increase the total reactivity of $j=0$ without changing the reactivity of the higher rotational states. We have already given a possible explanation of this rotational selective enhancement in terms of potential anisotropy in section IV.B. What we want to add here is that the difference between the SW and the SW-LR results reflects exactly the one between HSW and SW-LR-SO and, therefore, can be attributed to the different topology of the van der Waals wells.

If the three calculations which include the correction for the spin–orbit effect agree, we must look for the reason of the clear disagreement with the experiments in the common features of the three surfaces employed. As we have already stressed, the spin–orbit correction operates essentially at long-range and is negligible in the transition state region. This is supported by both *ab initio* and semi-empirical approaches. Therefore, the transition state of the reaction is essentially the same in all the investigations reported here. In the calculations which account for the spin–orbit effect, the potential energy surfaces employed correlate asymptotically with the proper electronic spin-orbit state $^2P_{3/2}$ of fluorine, while the uncorrected surface correlates with an unphysical state that is a statistical mixing of the two spin–orbit states.

The introduction of the correct asymptotic correlation increases the barrier of the reaction. Although such an increase in the barrier may appear appropriate, the fact that it leads to poor agreement with experiments indicates an inaccuracy of the transition state height in the original SW surface. In particular, from the good agreement of the calculations without spin–orbit correction, we can conclude that the inaccuracy of the transition state is of the order of one-third of the spin–orbit splitting of the fluorine atom, that is 0.39 kcal mol^{-1}.

V. Conclusions

Regarding the celebrated $F + H_2$ reaction as treated from the viewpoint of accurate quantum dynamics on the best available potential energy surface in the light of recent experimental integral and differential cross sections, this work points out the importance of describing accurately the potential energy surface not only in the transition state region, which is traditionally considered as the most determinant in reaction dynamics, but also in intermediate and long-range interaction regions, which can play a crucial role in the selectivity and in the angular distribution of the reaction products. This point has been also recently raised in the case of the Cl + HD reaction.[39] Spin–orbit effects are also found to play an important role in the reaction dynamics.

In this work fully converged quantum mechanical calculations for the $F + H_2$ reaction have been performed using a code based on an algorithm proposed and developed in our research group. A brief summary of the theoretical tools used in our hyperquantization algorithm has been given in Section III. Our results on the original SW surface are carefully compared with other well assessed calculations (see Section IV.A) to verify the reliability and the accuracy of our code.

Calculations on two new potential energy surfaces obtained by semi-empirical corrections at the entrance channel of the SW surface have been presented and compared with other theoretical studies to investigate the role of corrections in the long-range behavior. Two modifications of the entrance channel of the reaction have been considered: a more realistic description of the van der Waals well and of the long-range anisotropy of the potential and the spin–orbit effect, mainly affecting the height of the reaction barrier. A summary of the procedure used to build up the new surfaces has been given in Section II.

The excellent agreement of the total integral cross sections for our SW-LR-SO PES (including long-range and spin–orbit corrections) with the exact multisurface results of ref. 65 and with the adiabatic spin–orbit corrected calculations of ref. 48, supports the validity of the Born–Oppenheimer scheme, as a basis for the treatment of the dynamics of the title reaction. The obtained results are compared with three different sets of experimental data[3,31,36] regarding different features of the reaction dynamics. In some cases, better agreement between theory and experiments is found with respect to previous studies: in particular, differential cross sections and vibrational branching ratios appear to be sensitive to the long-range spin–orbit corrections. Specifically, the correct anisotropy of the potential in the entrance channel brings the calculated $v'=3$ ratios within the experimental error bars.

The modification of the van der Waals well does not alter significantly the shape of the differential cross sections but this conclusion is not expected to continue to be valid when other experiments involving lower collision energies are considered. The present dynamical approach can be extended to analyze the recent results described in ref. 80 and 81 as well as those in the ultracold regime where, however, experiments are lacking. Indeed, at very low collision energies, the dynamics is expected to be strongly influenced[82] by the long-range part of the potential and especially by the depth of the van der Waals well. Drastic changes in the resonance features[83,84] are anticipated. Further work in this direction is needed to evaluate the sensitivity to our proposed corrections of the dynamics in the collision energy range of the reaction threshold.

Proper allowance for the spin–orbit effect appears to lower the selective HF($v'=3$) forward peaks, in better agreement with experimental data. The incorrect trend of the total

integral cross sections with the collision energy must be attributed to some inaccuracy on the transition state region of the Stark–Werner surface. The good agreement found using the original PES without spin–orbit corrections suggests that the amount of such inaccuracy is an overestimation close to one third of the fluorine fine structure splitting. This is in agreement with ref. 57, where a similar conclusion was drawn from a rate constants study. In spite of much effort, the transition state for this reaction is still elusive, although now within only a fraction of a kcal mol^{-1}, and so the moral of the story appears to be not too different from that of the early review,[1] but is now substantiated by essentially exact quantum mechanical treatments of the dynamics.

Acknowledgments

We are grateful to F. Pirani, J. Castillo, M. B. Sevryuk, L. Y. Rusin, D. Nesbitt, M. Alexander and K. Liu for useful discussions and for communicating their results. D.D.F. is grateful to the Centre de Supercomputació de Catalunya (CESCA) and the Centre Europeu de Parallelisme de Barcelona (CEPBA) for supplying the CPU time used in the dynamical calculations and for the award of a grant within the E.U. Large Scale Facilities project of the Improving the Human Potential Programme (Contract No. HPRI-1999-CT-00071). We also thank D. Aragones Sabate of the CEPBA staff for help in parallelizing the computer code. The work in Perugia is supported by the Italian National Research Council (CNR), by the Ministero dell' Istruzione, dell' Universitá e della Ricerca (MIUR), by the European Union within the Human Potential Research Network "Theoretical Studies of Electronic and Dynamical Processes in Molecules and Clusters" [Contract No. HPRN-CT-1999-00005], by the COST D9 and D23 Action and by INTAS. The "Ente Nazionale Energia Alternativa" (ENEA) is also acknowledged.

References

1 H. F. Schaefer III, *J. Phys. Chem. A*, 1985, **89**, 5336.
2 D. E. Manolopoulos, *J. Chem. Soc., Faraday Trans.*, 1997, **93**, 673.
3 D. M. Neumark, A. M. Wodtke, G. N. Robinson, C. C. Hayden and Y. T. Lee, *J. Chem. Phys.*, 1985, **82**, 3045.
4 D. M. Neumark, A. M. Wodtke, G. N. Robinson, C. C. Hayden, R. Shobatake, R. K. Sparks, T. P. Schafer and Y. T. Lee, *J. Chem. Phys.*, 1985, **82**, 3067.
5 J. B. Anderson, *Adv. Chem. Phys.*, 1980, **41**, 229.
6 L. D. Hess, *J. Chem. Phys.*, 1971, **55**, 2466.
7 J. M. Launay and M. Le Dourneuf, *Chem. Phys. Lett.*, 1990, **169**, 476.
8 R. Steckler, D. G. Truhlar and B. C. Garrett, *J. Chem. Phys.*, 1985, **82**, 5499.
9 J. M. Launay, *Theor. Chim. Acta*, 1991, **79**, 183.
10 J. M. Launay and M. Le Dourneuf, Invited papers at *ICPEAC XVII Brisbane*, 1991, Adam Hilger, Bristol, 1992, p. 549.
11 F. B. Brown, R. Steckler, D. W. Schwenke, D. G. Truhlar and B. C. Garrett, *J. Chem. Phys.*, 1985, **82**, 188.
12 C. F. Bender, P. K. Pearson, S. V. O'Neil and H. F. Schaefer III, *J. Chem. Phys.*, 1972, **56**, 4626.
13 M. J. Frisch, B. Lin, J. S. Binkley, H. F. Schaefer III and W. H. Miller, *Chem. Phys. Lett.*, 1985, **114**, 1.
14 T. Takayanagi and S. Sato, *Chem. Phys. Lett.*, 1988, **144**, 191.
15 F. B. Brown and D. G. Truhlar, *Chem. Phys. Lett.*, 1985, **117**, 307.
16 R. Steckler, D. W. Schwenke, F. B. Brown and D. G. Truhlar, *Chem. Phys. Lett.*, 1985, **121**, 475.
17 D. W. Schwenke, R. Steckler, F. B. Brown and D. G. Truhlar, *J. Chem. Phys.*, 1986, **84**, 5706.
18 G. C. Lynch, R. Steckler, D. W. Schwenke, A. J. C. Varandas, D. G. Truhlar and B. C. Garrett, *J. Chem. Phys.*, 1991, **94**, 7136.
19 S. Mielke, G. Lynch, D. G. Truhlar and D. W. Schwenke, *Chem. Phys. Lett.*, 1993, **213**, 10.
20 K. Stark and H.-J. Werner, *J. Chem. Phys.*, 1996, **104**, 6515.
21 S. E. Bradforth, D. W. Arnold, D. M. Neumark and D. E. Manolopoulos, *J. Chem. Phys.*, 1993, **99**, 6345.
22 D. E. Manolopoulos, K. Stark, H.-J. Werner, D. W. Arnold, S. E. Bradforth and D. M. Neumark, *Science*, 1993, **262**, 1852.
23 A. Weaver, R. B. Metz, S. E. Bradforth and D. M. Neumark, *J. Chem. Phys.*, 1990, **93**, 5352.
24 A. Weaver and D. M. Neumark, *Faraday Discuss. Chem. Soc.*, 1991, **91**, 5.
25 J. F. Castillo, D. E. Manolopoulos, K. Stark and H. Werner, *J. Chem. Phys.*, 1996, **104**, 6531.
26 F. J. Aoiz, L. Banares, V. J. Herrero, V. Saez Rabanos, K. Stark and H.-J. Werner, *Chem. Phys. Lett.*, 1994, **223**, 215.
27 F. J. Aoiz, L. Bañares, B. Martínez-Haya, J. F. Castillo, D. Manolopoulos, B. Hartke and H.-J. Werner, *J. Phys. Chem. A*, 1997, **101**, 6403.
28 A. J. Dobbyn, P. McCabe, J. N. L. Connor and J. F. Castillo, *Phys. Chem. Chem. Phys.*, 1999, **1**, 11.
29 D. Sokolovsky and J. F. Castillo, *Phys. Chem. Chem. Phys.*, 2000, **2**, 507.
30 R. T. Skodje, D. Skouteris, D. Manolopoulos, S. H. Lee, F. Dong and K. Liu, *J. Chem. Phys.*, 2000, **112**, 4536.
31 F. Dong, S.-H. Lee and K. Liu, *J. Chem. Phys.*, 2000, **113**, 3633.
32 M. Faubel, L. Y. Rusin, S. Schlemmer, F. Sondermann, U. Tappe and J. P. Toennies, *J. Chem. Phys.*, 1994, **101**, 2106.
33 M. Faubel, B. Martínez-Haya, L. Y. Rusin, U. Tappe and J. P. Toennies, *Chem. Phys. Lett.*, 1995, **232**, 197.
34 M. Faubel, B. Martínez-Haya, L. Y. Rusin, U. Tappe and J. P. Toennies, *J. Phys. Chem. A*, 1997, **101**, 6415.
35 W. B. Chapman, B. W. Blackmon and D. J. Nesbitt, *J. Chem. Phys.*, 1997, **107**, 8193.
36 W. B. Chapman, B. W. Blackmon, S. Nizkorodov and D. J. Nesbitt, *J. Chem. Phys.*, 1998, **109**, 9306.
37 G. Dharmasena, T. R. Phillips, K. N. Shokhirev, G. A. Parker and M. Keil, *J. Chem. Phys.*, 1997, **106**, 9950.
38 G. Dharmasena, K. Copeland, J. H. Young, R. A. Lasell, T. R. Phillips, G. A. Parker and M. Keil, *J. Phys. Chem. A*, 1997, **101**, 6429.
39 D. Skouteris, D. E. Manolopoulos, W. Bian, H.-J. Werner, L.-H. Lai and K. Liu, *Science*, 1999, **286**, 1713.
40 V. Aquilanti, R. Candori, D. Cappelletti, E. Luzzatti and F. Pirani, *Chem. Phys.*, 1990, **145**, 293.
41 V. Aquilanti, D. Cappelletti and F. Pirani, *J. Chem. Soc., Faraday Trans.*, 1993, **89**, 1467.
42 V. Aquilanti, S. Cavalli, F. Pirani, A. Volpi and D. Cappelletti, *J. Phys. Chem. A*, 2001, **105**, 2401.
43 T. W. J. Whiteley, A. J. Dobbyn, J. N. L. Connor and G. C. Schatz, *Phys. Chem. Chem. Phys.*, 2000, **2**, 549.
44 V. Aquilanti, S. Cavalli and D. De Fazio, *J. Chem. Phys.*, 1998, **109**, 3792.
45 V. Aquilanti, S. Cavalli, D. De Fazio and A. Volpi, *Adv. Quantum Chem.*, 2001, **39**, 103.
46 P. Palmieri, C. Puzzarini, V. Aquilanti, G. Capecchi, S. Cavalli, D. De Fazio, A. Aguilar, X. Giménez and J. M. Lucas, *Mol. Phys.*, 2000, **98**, 1835.
47 V. Aquilanti, S. Cavalli, D. De Fazio and A. Volpi, *Int. J. Quantum Chem.*, 2001, **85**, 368.
48 J. F. Castillo, B. Hartke, H.-J. Werner, F. J. Aoiz, L. Bañares and B. Martínez-Haya, *J. Chem. Phys.*, 1998, **109**, 7224.
49 B. Hartke and H.-J. Werner, *Chem. Phys. Lett.*, 1997, **280**, 430.
50 M. Faubel, L. Y. Rusin, S. Schlemmer, F. Sondermann, U. Tappe and J. P. Toennies, *J. Chem. Soc., Faraday Trans.*, 1993, **89**, 1475.
51 F. A. Gianturco, F. Ragnetti, M. Faubel, B. Martínez-Haya, L. Y. Rusin, F. Sondermann and U. Tappe, *Chem. Phys.*, 1995, **200**, 405.
52 M. Ayabakan, M. Faubel, B. Martínez-Haya, L. Yu. Rusin, M. B. Sevryuk, U. Tappe and J. P. Toennies, *Chem. Phys.*, 1998, **229**, 21.
53 V. Aquilanti and G. Grossi, *J. Chem. Phys.*, 1990, **73**, 1165.
54 J. Andres, U. Buck, F. Huisken, J. Schleusener and F. Torello, *J. Chem. Phys.*, 1980, **73**, 5620.
55 U. Buck, *Faraday Discuss. Chem. Soc.*, 1982, **73**, 187.
56 S. Nizkorodov, W. W. Harper, W. B. Chapman, B. W. Blackmon and D. J. Nesbitt, *J. Chem. Phys.*, 1999, **111**, 8404.
57 F. J. Aoiz, L. Bañares and J. F. Castillo, *J. Chem. Phys.*, 1999, **111**, 4013.
58 E. Rosenman, S. Hochman-Kowal, A. Persky and M. Baer, *Chem. Phys. Lett.*, 1996, **257**, 421.
59 D. De Fazio and J. F. Castillo, *Phys. Chem. Chem. Phys.*, 1999, **1**, 1165.
60 F. Rebentrost and W. A. Lester, Jr., *J. Chem. Phys.*, 1975, **63**, 3737.
61 F. Rebentrost and W. A. Lester, Jr., *J. Chem. Phys.*, 1976, **64**, 3879.

62 F. Rebentrost and W. A. Lester, Jr., *J. Chem. Phys.*, 1977, **67**, 3367.
63 M. Gilibert and M. Baer, *J. Phys. Chem.*, 1994, **98**, 12 822.
64 G. D. Billing, L. Y. Rusin and M. B. Sevryuk, *J. Chem. Phys.*, 1995, **103**, 2482.
65 M. H. Alexander, D. E. Manolopoulos and H.-J. Werner, *J. Chem. Phys.*, 2000, **113**, 11 084.
66 P. Honvault and J. M. Launay, *Chem. Phys. Lett.*, 1999, **303**, 657.
67 V. Aquilanti, S. Cavalli, D. De Fazio, A. Volpi, A. Aguilar, X. Gimenez and J. M. Lucas, *J. Chem. Phys.*, 1998, **109**, 3805.
68 V. Aquilanti, S. Cavalli and D. De Fazio, *J. Phys. Chem.*, 1995, **99**, 15 964.
69 V. Aquilanti, S. Cavalli, D. De Fazio, A. Volpi, A. Aguilar, X. Gimenez and J. M. Lucas, *Phys. Chem. Chem. Phys.*, 1999, **1**, 1091.
70 T. Ericsson and A. Ruhe, *Math. Comput.*, 1980, **35**, 1251.
71 B. R. Johnson, *J. Comput. Phys.*, 1973, **14**, 445.
72 D. E. Manolopoulos, *J. Chem. Phys.*, 1986, **85**, 6425.
73 N. Balucani, L. Cartechini, P. Casavecchia, G. G. Volpi, F. J. Aoiz, L. Bañares, M. Menéndez, W. Bian and H.-J. Werner, *Chem. Phys. Lett.*, 2000, **328**, 6253.
74 V. Aquilanti, S. Cavalli, G. Grossi and R. W. Anderson, *J. Phys. Chem.*, 1991, **95**, 8184.
75 R. W. Anderson, V. Aquilanti, S. Cavalli and G. Grossi, *J. Phys. Chem.*, 1993, **97**, 2243.
76 J. M. Alvariño, V. Aquilanti, S. Cavalli, S. Crocchianti, A. Laganá and T. Martínez, *Chem. Phys.*, 1997, **107**, 3339.
77 J. M. Alvariño, V. Aquilanti, S. Cavalli, S. Crocchianti, A. Laganá and T. Martínez, *J. Phys. Chem. A*, 1998, **102**, 9638.
78 J. F. Castillo and D. E. Manolopoulos, *Faraday Discuss.*, 1998, **110**, 119 and related dicussion.
79 S. A. Nizkorodov, W. W. Harper and D. J. Nesbitt, *Faraday Discuss.*, 1999, **113**, 107 and related dicussion.
80 M. Baer, M. Faubel, B. Martínez-Haya, L. Y. Rusin, U. Tappe and J. P. Toennies, *J. Chem. Phys.*, 1999, **110**, 10 231.
81 L. Y. Rusin and J. P. Toennies, *Phys. Chem. Chem. Phys.*, 2000, **2**, 501.
82 N. Balakrishnan and A. Dalgarno, *Chem. Phys. Lett.*, 2001, **341**, 652.
83 T. Takayanagi and Y. Kurosaki, *J. Chem. Phys.*, 1998, **109**, 8929.
84 T. Takayanagi and Y. Kurosaki, *Chem. Phys. Lett.*, 1998, **286**, 35.